A non-reference evaluation method for edge detection of wear particles in ferrograph images

CrossMark

Jingqiu Wang, Ju Bi, Lianjun Wang, Xiaolei Wang *

Nanjing University of Aeronautics and Astronautics, Nanjing 210016, China

A R T I C L E   I N F O

A B S T R A C T

Edges are one of the most important features of wear particles in a ferrograph image and are widely used to extract parameters, recognize types of wear particles, and assist in the identification of the wear mode and severity. Edge detection is a critical step in ferrograph image processing and analysis. Till date, there has been no single algorithm that guarantees the production of good quality edges in ferrograph images for a variety of applications. Therefore, it is desirable to have a reliable evaluation method for measuring the performance of various edge detection algorithms and for aiding in the selection of the optimal parameter and algorithm for ferrographic applications. In this paper, a new non-reference method for the objective evaluation of wear particle edge detection is proposed. In this method, a comprehensive index of edge evaluation is composed of three components, i.e., the reconstruction based similarity sub-index between the original image and the reconstructed image, the confidence degree sub-index used to show the true or false degree of the edge pixels, and the edge form sub-index that is used to determine the direction consistency and width uniformity of the edges. Two experiments are performed to illustrate the validity of the proposed method. First, this method is used to select the best parameters for an edge detection algorithm, and it is then used to compare the results obtained using various edge detection algorithms and determine the best algorithm. Experimental results of various real ferrograph images verify the effectiveness of the proposed method.

1. Introduction

With the development of modern mechanical equipment in the direction of large scale, high productivity, and high reliability, predictive maintenance procedures based on the machine conditions are necessary for decreasing the occurrence of over-maintenance as well as to prevent the sudden breakdown of machines. Ferrography has been proven to be an effective means of wear-condition monitoring and fault diagnosis of machines such as aero-engines and mining equipment. This technique is used to determine the wear condition and wear mechanisms of machines through qualitative and quantitative analysis on the amount, size, shape, colour, and texture of the wear particles (wear debris) contained in the lubricating or hydraulic system [1,2]. However, the dependency on human expertise for the analysis and interpretation limits the application and potential of this method in the industry [3]. The development of computer image analysis could provide a solution for the aforementioned problems and greatly improve the accuracy and efficiency of ferrograph analysis [4,5].

---

* Corresponding author.
  E-mail address: wxl@nuaa.edu.cn (X. Wang).

In the last three decades, many efforts have been focused on the application of image processing techniques for the feature extraction and classification of wear particles [6–11]. Analysis systems based on human–computer interaction, such as the CAVE [12], CASPA [13], and SYCLOPS [14], as well as expert systems based on 3D particle analysis [15] have been developed.

CAVE is an interactive control system that is mostly used to carry out analysis on single particles. It applies Fourier transforms and the curvature analysis of the outline of a particle as the input parameters into a neural network, which then classifies the particle's shape.

CASPA was developed as an off-line debris classifier. The user is prompted to answer a series of text-based questions concerning the morphology of the particle. Then, it classifies the wear particles in terms of the wear mode by using an expert system.

SYCLOPS is a semi-automated wear-debris classification system. It classifies the characteristics of the particles by matching them to a selection of stylized images. For example, by defining the particle's shape as regular, irregular, or elongated, the user can determine which corresponding image resembles the shape of the particle.

Peng et al. developed an expert system based on 3D particle analysis for interpreting the analysis data of wear debris to assist machine-condition monitoring and fault diagnosis. However, it is difficult to obtain 3D image analysis data in most application fields.

Recently, efforts have been made to develop an automatic and reliable wear particle analysis system [16,17]. The application of such systems should significantly reduce the inspection time and the requirement of the inspector's expertise [18]. In such an automatic system, wear particles are first segmented from each other, then the features and parameters are extracted, and finally, the wear particles are classified and recognized based on the extracted features.

Edges are one of the most important features of wear particles in a ferrograph image, and they provide a concise and accurate representation of the wear particle boundaries. From the edges, more complicated features and parameters of the wear particles can be extracted. For example, the parameters of area, perimeter, and aspect ratio help in classifying the type of wear particles and subsequently, the wear mode and severity.

Edge detection is a fundamental operation performed in lower-level image processing and computer vision systems. Popular edge detection algorithms or detectors include the Sobel, Robert, Prewitt, Laplacian, LoG, and Canny [19]; currently, the wavelet [20], grey relational operator [21], and marker-watershed algorithms [22] are also applied for the edge detection of wear particles.

Although the performance of the majority of edge detectors is acceptable for simple and noise-free images, the case is different for ferrograph images. For various practical environments, the size, colour, and noise of ferrograph images are very different, which significantly increases the complexity involved in edge detection. It is known that the appearance of the edges of wear particles in an image varies greatly. The edges vary with respect to the types of wear particles and their shapes in the images. The edges may be crowded, blurred, or sparse. After the edge detection, the edge image may still contain some isolated edge points or broken segments. Fig. 1(a) shows an original ferrograph image containing wear particles of various sizes, outlines, brightness, and surface textures. Fig. 1(b)–(d) show the results of the edge detection performed using the Sobel, LoG, and Canny detector, respectively. When the Sobel detector is used, as shown in Fig. 1(b), it generates several false edges for the particles with textures on their surfaces, and the edges of the wear particles are not single-pixel-wide. When using the LoG detector, some edges tend to be lost owing to blurring, and it also generates several false edges, as shown in Fig. 1(c). When using the Canny detector, the edges are detected single-pixel-wide; however, the blurred edges are lost, which results in a discontinuous and unclosed outline of wear particles, as shown in Fig. 1(d).

Till date, there has been no single detection algorithm that guarantees the production of good quality edges in ferrograph images for a variety of applications. Therefore, it is desirable to have a reliable evaluation method for measuring the performance of various edge detection algorithms and for aiding the selection of the optimal parameter and algorithm for ferrographic applications.

The types of edge evaluation methods can be divided into subjective and objective evaluations. Subjective evaluation usually involves the evaluation of edge detectors by observers; however, it is inevitably expensive with respect to time and

(a) Original image   (b) Sobel   (c) LoG   (d) Canny
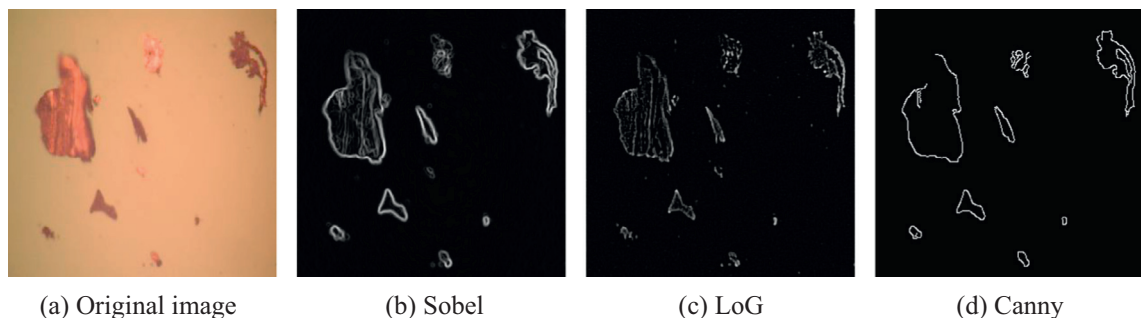
Fig. 1. Typical ferrograph image and results of edge detection.

resources, and difficult to automate [23]. Objective evaluation can be classified as reference-based [24,25] and non-reference-based methods [26]. In the reference-based method, a ground truth image is required as a reference in order to evaluate its similarity to the candidate edge maps. However, the ground truth image is not available for ferrograph images because of the diversity of wear particles. The non-reference-based method does not require a ground truth image. It uses information from the detected edge map and the original image itself to perform the aforementioned evaluation. Furthermore, most importantly, the non-reference-based method can be automated and is suitable for intelligent ferrography analysis. An objective evaluation method can play a variety of roles in image processing applications. It can not only be used to dynamically monitor the detection quality but also to optimize algorithms and the parameter settings of image processing systems. For example, the objective and quantitative evaluation method can be used as an online feedback signal supplied to the iterative processes of the edge detection of wear particles. It can also be used to provide support for selecting a better edge detector or a set of better operator parameters.

Therefore, in this paper, a new non-reference method for the objective evaluation of wear particle edges is proposed. In this method, the comprehensive index of edge evaluation is composed of three components. The first component is the reconstruction based similarity sub-index between the original image and the reconstructed image. The second component is the confidence degree sub-index, which is used to indicate the true or false degree of the edge pixels. The third component is the edge form sub-index, which is used to indicate the direction consistency and width uniformity of the edges. Two experiments are performed to illustrate the validity of the proposed algorithm. In the first experiment, this method is used to select the best parameters in an edge detection algorithm. In the second experiment, this method is used to compare the result of various edge detection algorithms and determine the best result.

2. Non-reference evaluation method of edge detection

In this paper, a non-reference evaluation method of edge detection is presented based on three indices, namely the reconstruction similarity sub-index, confidence degree sub-index, and edge form sub-index. A block diagram and the intermediate results of the proposed evaluation method is shown in Fig. 2.

2.1. Reconstruction similarity sub-index

The reconstruction similarity sub-index is used to compare the reconstructed and original images. The theoretical basis of this method is that a good edge map captures the essential structures and details of the original images. Therefore, using the pixel information, a reconstruction on a better edge map would be more similar to the original image [26].

2.1.1. Reconstruction process

Carlsson [27] proposed a method for reconstructing the image based on the detected edges. The basic principle is to reconstruct the image based on the pixels on both sides of the edge. Interpolation has been used to help reconstruct the edge image from the original image. Let I, E, and E_D represent the original image, binary edge image after edge detection, and the image obtained after the application of morphology dilation on E, respectively. Let E_T represent the edge tube image, which is obtained by using the "AND" operation between I and E_D, i.e.,

if $E_D(i,j) = 1$, then $E_T(i,j) = I(i,j)$,
else, if $E_D(i,j) = 0$, then $E_T(i,j) = 0$.

If R represents a reconstructed image, under the constraints $R(i,j) = E_T(i,j)$ and $E_D(i,j) = 1$, the Carlsson reconstruction method can be described as
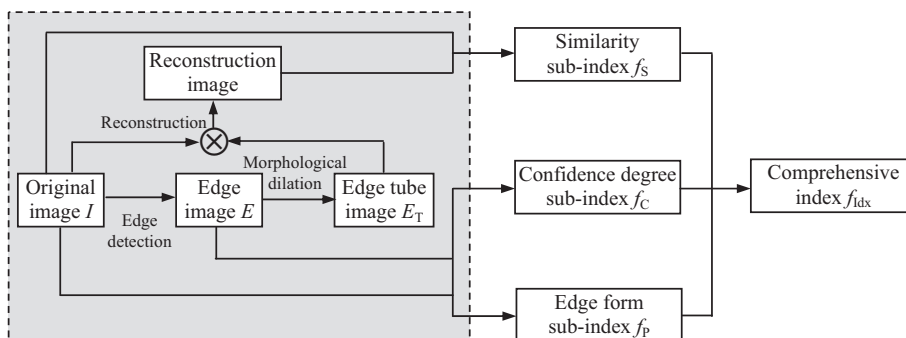
Fig. 2. Block diagram of the evaluation method.

$$\min\left(\iint\left(\frac{\partial R}{\partial i}\right)^2+\left(\frac{\partial R}{\partial j}\right)^2 d_i d_j\right). \tag{1}$$

i.e., the reconstruction of the image comprises the minimization of the above function.

Based on the Carlsson method, Govindarajan et al. proposed an eight-direction linear-interpolation reconstruction method and a weighted-median reconstruction method [28,29].

As shown in Fig. 3(a), $A(i,j)$ is one of the background pixels in E_T. By searching in all eight directions (horizontal, vertical, and diagonal) in E_T, the edge pixel T_k ($k = 1, 2, \ldots, 8$), which is the nearest to pixel A in each direction can be found. Let t_k ($k = 1, 2, \ldots, 8$) represent the grey value of the corresponding edge pixels, and d_k ($k = 1, 2, \ldots, 8$) represent the distance between T_k ($k = 1, 2, \ldots, 8$) and A. Thus, the linear interpolation reconstruction formula of pixel A is

$$R(i,j)=\frac{\sum_{k=1}^{8}(t_k/d_k)}{\sum_{k=1}^{8}(1/d_k)}. \tag{2}$$

The weighted median reconstruction formula is

$$R(i,j)=median(t_1\diamond w_1,t_2\diamond w_2,\ldots,t_8\diamond w_8), \tag{3}$$

where

$$w_k=round(100/d_k), \tag{4}$$

and $\diamond$ is the replicator operator, which is defined as

$$t\diamond w=\underbrace{(t,t,\ldots,t)}_{w}. \tag{5}$$

The distance between two pixels in a direction influences the reconstruction result. Shepherd [30] pointed out that, in psychological space, the probability of generalization approximates an exponential decay function of distance. Jin et al. [31] proposed a weighted formula, which describes the decay as

$$w=1.0-\frac{1.0}{(1.0+e^d)^{3.75}}, \tag{6}$$

where w belongs to $[0, 1]$.

According to human visual psychology, the pixels nearer to the reconstructed pixel will have a relatively large impact on it. Therefore, in our method, on considering the reconstruction pixel as the centre, its neighbourhood is divided into eight regions, as shown in Fig. 3(b). Two pixels in each region, which have the nearest distance to the centre pixel, are located. The two pixels are represented as t_{kj} ($k = 1, 2, \ldots, 8; j = 1, 2$). The reconstruction equation based on the psychological distance is

$$R(i,j)=\frac{\sum_{k=1}^{8}\sum_{j=1}^{2}(t_{k,j}/w_{k,j})}{\sum_{k=1}^{8}\sum_{j=1}^{2}(1/w_{k,j})}. \tag{7}$$
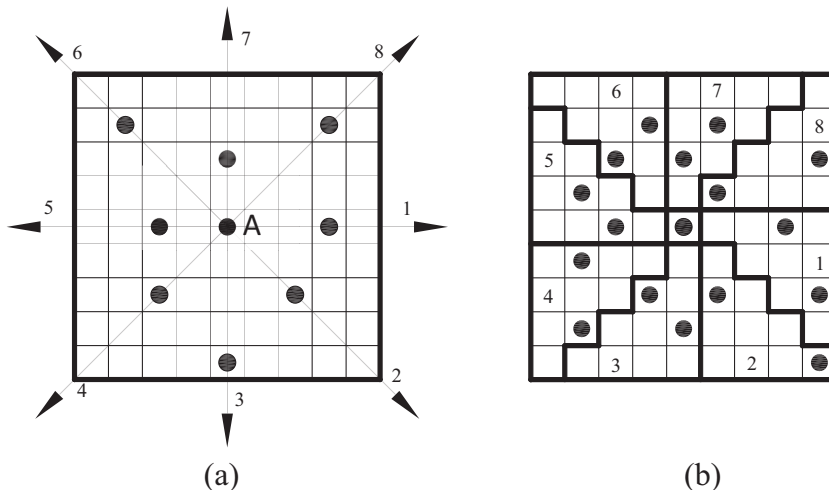
Fig. 3. Interpolation mode of image reconstruction.

The improved reconstruction method uses eight regions instead of the eight standard directions in the traditional method, and the psychological distance is also introduced to the pixel distance, which is in line with human visual psychology; a more accurate reconstructed image could thus be obtained.

Fig. 4 shows an example of image reconstruction, where Fig. 4(a) is a local image of a wear particle, and Fig. 4(b) shows a binary edge image after edge detection. Fig. 4(c) shows the grey value of each pixel in the edge tube image, and Fig. 4(d) shows the grey value of the corresponding pixels after image reconstruction.

2.1.2. Reconstruction similarity

The accuracy of the edge detection can be evaluated by determining the similarity between the original image and the reconstructed image.

For determining the similarity between two images, the pixel-wise mean square error (MSE) and mean absolute error (MAE) are the most commonly adopted statistical methods. A lower MSE or MAE indicates a greater similarity between two images and a superior quality of edge detection. However, these statistical methods do not take the human visual system properties into consideration. Therefore, they are inappropriate for use as reliable measures for some images [26]. Wang et al. [32] proposed a similarity evaluation method that defines the similarity of two images as a function of luminance, contrast, and structure.

Given two images x and y, μ_x and μ_y represent the mean of the grey value of each image; σ_x and σ_y represent the standard deviation of the grey value of image x and y, respectively; and σ_{xy} represents the covariance of image x and y. c_1, c_2, and c_3 are constant values. The similarity of the two images is defined as

$$SSIM(x,y) = \frac{(2\mu_x\mu_y + c_1)(2\sigma_{xy} + c_2)}{(\mu_x^2 + \mu_y^2 + c_1)(\sigma_x^2 + \sigma_y^2 + c_2)}, \tag{8}$$

where

$$c_1 = (K_1 L)^2,$$

$$\mu_x = \sum_{i=1}^{N} w_i x_i,$$

$$\sigma_x = \left(\sum_{i=1}^{N} w_i (x_i - \mu_x)^2 \right)^{1/2},$$

$$\sigma_{xy} = \sum_{i=1}^{N} w_i (x_i - \mu_x)(y_i - \mu_y).$$

(a) Local image and pixel value

57	57	57	61	87	120
57	57	59	72	106	123
59	59	64	90	122	124
61	64	89	117	124	124
68	89	114	125	124	124
89	114	128	125	125	125

(b) Edge image and pixel value

0	0	0	0	255	0
0	0	0	0	255	0
0	0	0	255	0	0
0	0	255	0	0	0
0	255	0	0	0	0
255	0	0	0	0	0

(c) Edge tube image and pixel value

0	0	0	61	87	120
0	0	0	72	106	123
0	0	64	90	122	0
0	64	89	117	0	0
68	89	114	0	0	0
89	114	0	0	0	0

(d) Reconstruction image and pixel value

63	65	57	61	87	120
64	68	59	72	106	123
68	59	64	90	122	124
61	64	89	117	124	121
68	89	114	125	124	124
89	114	128	125	124	123

Fig. 4. Reconstruction of wear particle image.

J. Wang et al./Mechanical Systems and Signal Processing 100 (2018) 863–876

The reconstruction similarity sub-index over the entire image is defined as the mean of the SSIM values

$$f_S = MSSIM = \frac{1}{mn}\sum_{i=1}^{m}\sum_{j=1}^{n}SSIM(x_i, y_i). \tag{9}$$

It can be seen from Eq. (9) that the entire image of the reconstruction similarity f_s is a monotone function, and therefore, the greater the number of detected edge pixels, the greater the reconstructed similarity will be. However, it is obvious that the reconstruction image will have a large similarity with the original image if the edge image has more pixels including false edge pixels; unfortunately, the quality of the edge detection is not very good. Therefore, it is necessary to identify and distinguish between authentic and false edge pixels.

2.2. Confidence degree sub-index

Because of the texture on the surface of some wear particles or the blurred edges of some thick particles, some false edges may be detected; hence, it is necessary to evaluate the authenticity of the edge pixels.

The grey value of an edge pixel is different from its neighbouring pixels, and thus, the mean square deviation of the grey value of the edge pixel and its neighbour can be used to indicate this difference.

In order to reduce the interference of the noise, the neighbouring mean square deviation of a pixel is calculated from the average grey value of its neighbouring pixels while excluding the pixel that has the maximum or minimum grey value in the neighbourhood.

For pixel $I(i, j)$, its $k \times k$ neighbourhood is defined as

$$Iw_{i,j} = \{I(x, y); x - i = 0, \pm 1, \ldots, \pm(k-1)/2; y - j = 0, \pm 1, \ldots, \pm(k-1)/2\}.$$

Thus, the mean square deviation is

$$\sigma_{i,j} = \sqrt{\frac{1}{k^2 - 2}\sum_{\substack{I(x,y)\in Iw_{i,j} \\ I(x,y)\notin max(Iw_{i,j}) \\ I(x,y)\notin min(Iw_{i,j})}} (I(x, y) - \mu_{i,j})^2} \tag{10}$$

where $\mu_{i,j}$ is the mean gray value of the remaining pixels after the two pixels that have the maximum and minimum grey values are eliminated. The neighbouring mean grey deviation of pixel $I(i, j)$ in the original image $I(m \times n)$ is defined as

$$\sigma_{i,j}^I; \ i = 1, \ldots, m; \ j = 1, \ldots, n.$$

The neighbouring mean grey deviation of the edge pixel $E(i, j)$ in the original image is defined as

$$\sigma_{i,j}^E, \quad E(i,j) = 1; \ i = 1, \ldots, m; j = 1, \ldots, n.$$

In the $k \times k$ neighbourhood of an edge pixel $E(i, j)$, the automatic threshold method is used to separate the background from the edge pixels, and then, the number of the background pixels N can be determined. The maximum mean grey deviation in the neighbourhood of the edge pixel $E(i, j)$ can be obtained as

$$T_{\sigma_{i,j}}^E, \quad E(i,j) = 1; \ i = 1, \ldots, m; j = 1, \ldots, n.$$

Therefore, the relative grey deviation of the edge pixel $E(i, j)$ is defined as

$$\sigma_{i,j}' = \begin{cases} \sigma_{i,j}^E / T_{\sigma_{i,j}}^E, & N > N_0 \\ 0, & N \leqslant N_0 \end{cases}, \tag{11}$$

where N_0 is a constant, and generally, if $k = 7$, $N_0 = 20$.

A larger relative deviation corresponds to a more significant change in the grey value in the neighbourhood of pixel $E(i, j)$, and subsequently, the higher relative authenticity of $E(i, j)$ as the edge pixel. Conversely, a smaller relative deviation corresponds to a smaller change in the grey value and a higher relative possibility that $E(i, j)$ is a false edge pixel.

The confidence degree sub-index of a pixel is defined as

$$c_{i,j} = f(\sigma_{i,j}') = \begin{cases} \frac{1 + \sqrt{2\sigma_{i,j}' - 1}}{2}, & \sigma_{i,j}' \geqslant 0.5 \\ 2\sigma_{i,j}'^2, & \sigma_{i,j}' < 0.5 \end{cases}. \tag{12}$$

The confidence degree sub-index of the edge image is the mean value of that of all the edge pixels.

$$f_C = \frac{1}{sum}\sum_{E(i,j)=1} c_{i,j}, \tag{13}$$

where sum is the number of the detected edge pixels.

In general, the greater the number of edge pixels that are detected, the greater the probability that the false edges appear, and the smaller the edge confidence is. To a certain extent, the reconstructed similarity sub-index could be corrected by using the confidence degree sub-index.

2.3. Edge form sub-index

The edge form indicates the edge connectivity and the edge width uniformity [33]. The edge connectivity measures how edge pixels are contiguous and edge segments are connected. The edge width uniformity evaluates how the edges are formed as thin lines.

Let $E(m,n)$ denote an edge image obtained from the edge detection, and $E_p(x,y)$ denote an edge pixel. For an edge pixel, $E_p(x,y) = 1$, and for a non-edge pixel, $E_p(x,y) = 0$. Let $W_d(E_p(x,y))$ be an evaluation window the size of which is $d \times d$, and $E_p(x,y)$ is located at the center of the window. Let $P_d(k)$ denote the pixel patterns that are formed by k edge pixels in $W_d(E_p(x,y))$, where $k < d^2$. That is, a $P_d(k)$ pattern has k edge pixels in a square window consisting of $d \times d$ image pixels, with the evaluating edge pixel at the centre. As the k edge pixels can be distributed in various ways in the $d \times d$ window, $P_d(k)$ actually represents a group of pixel patterns. Let $P_d^i(k)$ denote the individual edge patterns in the $P_d(k)$ group. Let $|P_d(k)|$ be the number of individual edge patterns in the $P_d(k)$ pattern group, and $\#P_d^i(k)$ be the total number of occurrences of $P_d^i(N)$ edge patterns in an image. Let N be the total number of edge pixels in an image $E(m,n)$.

$$|P_d(k)| = C(d^2 - 1, k - 1). \tag{14}$$

The strength value $S(P_d(k))$ for a pattern group $P_d(k)$ is

$$S(P_d(k)) = \frac{1}{|P_d(k)|} \sum_{i=1}^{|P_d(k)|} S(P_d^i(k)). \tag{15}$$

On considering an evaluation window of size 3×3 as an example, the strength value $S(P_3(k))$ for a pattern $P_d(k)$ is shown in Table 1 [33].

It can be seen from Table 1 that when there are three to five edge pixels in the evaluation window of size 3×3, the strength values are relatively large, and thus these pixels would be true edge pixels. If there are only one to two pixels in the window, the strength value is small, and these pixels are noise in the image. When the detected window has more than six pixels, the strength value is small, which means that the pixels may be located on the blurred edges.

The edge form sub-index f_P of the edge image is defined as the mean value of the strength of each edge pixel.

$$f_P = \mu_s(E(m,n)) = \frac{1}{N} \sum_{k=1}^{d^2} \#P_d(k) * S(P_d(k)). \tag{16}$$

The range of f_P is $[0,1]$, a higher f_P represents a better quality of edge detection.

2.4. Comprehensive index

Based on the characteristics and relationships of the above three indices, this paper presents a comprehensive index f_{Idx} that can be used to objectively evaluate the quality of edge detection of the wear particle image

$$f_{Idx} = f_S \times f_C \times f_P. \tag{17}$$

These three indices, namely, the reconstruction similarity sub-index f_s, the confidence degree sub-index f_c, and the edge form sub-index f_p are all in the range of 0–1, and therefore, the range of the comprehensive evaluation index is also in the range of 0–1.

When the parameters in an edge detection algorithm are changed or a different edge detection algorithm is applied to detect the edges of wear particles in ferrograph images, a different result is obtained. The greater the number of detected edge pixels, the larger the reconstruction similarity sub-index, and the smaller the confidence degree sub-index. The edge form sub-index is used to correct the reconstruction similarity sub-index and confidence degree sub-index in a manner similar to that of a normal function, which can guarantee a more accurate comprehensive evaluation index.

Table 1
Strength value and the normalization strength value [33].

k	1	2	3	4	5	6	7	8	9
$P_3(k)$	1	8	28	56	70	56	28	8	1
$S(P_3(k))$	0	0.50	0.86	0.89	0.71	0.36	0.07	0	0
Normalization $S(P_3(k))$	0	0.56	0.97	1.00	0.80	0.40	0.08	0	0

3. Experiments and results

The objectives of the experiments include two aspects: the performance of the edge detection algorithm with various parameters is evaluated in order to realize the optimization of the parameters of the algorithm, and various edge detection algorithms are compared using the same ferrograph image in order to evaluate the various edge detection algorithms. The experimental ferrograph images are obtained from petrochemical equipment. The image size is 300×300 pixels. The proposed algorithm is developed based on VC++ 6.0 and OpenCV 1.0 platform.

3.1. Evaluation of an edge detection algorithm using various parameters

Several efforts have been focused on the edge detection of wear particles. Fig. 5(a) shows a ferrograph image with some abnormal large wear particles and small debris. Fig. 5(b)–(g) show the various results obtained on using the L&G edge detection algorithm [34] on the ferrograph image shown in Fig. 5(a). The L&G algorithm makes use of two parameters: one parameter is the threshold of the wavelet analysis, and the other is the double parameters of the threshold of the grey relational analysis. Six groups of the combinations used are shown in Table 2.

By using the above six groups of thresholds, various edge images can be obtained, as shown in Fig. 5(b)–(g). The evaluation method with the proposed comprehensive index is applied to these images, and the evaluation results are shown in Table 3.

It could be observed from Fig. 5(b)–(d) that only some isolated pixels are detected, which are not connected to present the real edges. Fig. 5(e) and (f) show partially complete edges of the wear particles; however, some of the edges are unclosed. Fig. 5(g) shows the best edge detection result—most of the edges are detected and they are closed, with single-pixel-wide.

The larger the comprehensive index, the better the edge image obtained. As can be observed from Table 3, the order of the quality of the evaluation result is

Fig. 5(g) > Fig. 5(f) > Fig. 5(e) > Fig. 5(d) > Fig. 5(c) > Fig. 5(b).

The evaluation result is the same as that observed with human eyes.

When the parameters are set as per group 6, i.e., (0.15, (0.83, 0.98)), the best edge detection result is obtained. At the same time, from the comparison of the evaluation results of Fig. 5(e) and (g), it can be observed that the change in wavelet parameters has little effect on the comprehensive index f_{Idx}. However, if the parameter of the grey relational analysis is changed, for example, the different parameter of Fig. 5(d) and (g), the comprehensive index f_{Idx} is also changed accordingly. Therefore, in the L&G edge detection algorithm, the parameter of the grey relational analysis has a greater effect on the edge detection

(a) Original image   (b) f_{Idx} = 0.278   (c) f_{Idx} = 0.287   (d) f_{Idx} = 0.294

(e) f_{Idx} = 0.591   (f) f_{Idx} = 0.604   (g) f_{Idx} = 0.619
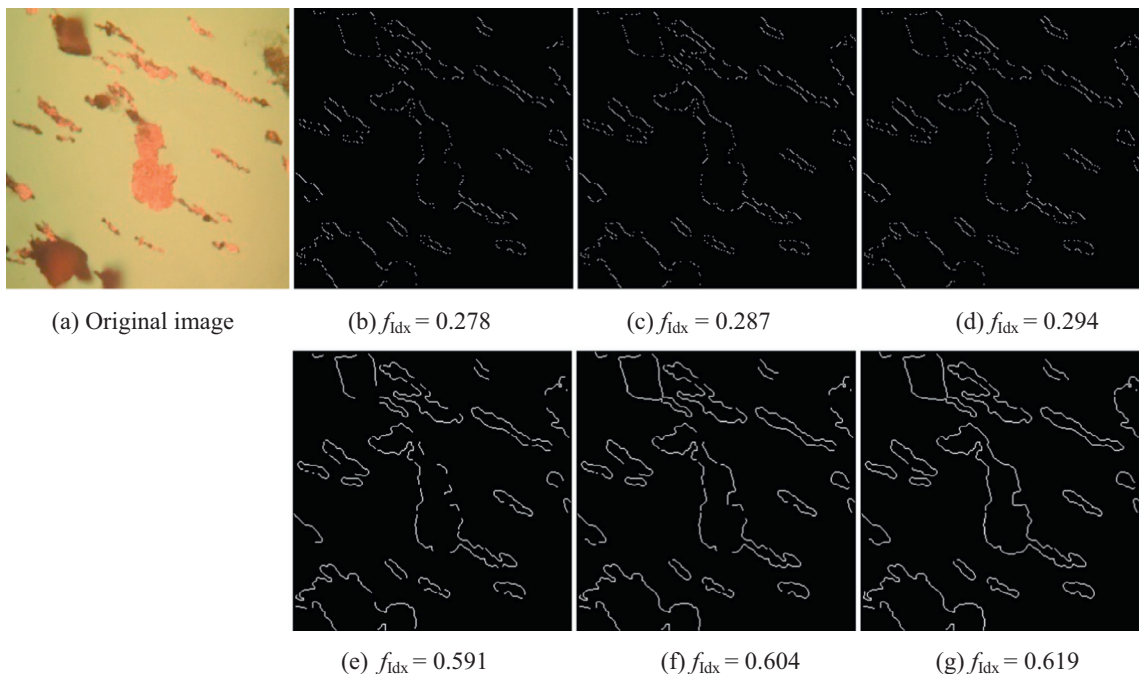
Fig. 5. Edge images of example 1 obtained with different parameter values.

Table 2
Combinations of the parameters of L&G algorithm.

Threshold	Group 1	Group 2	Group 3	Group 4	Group 5	Group 6
Wavelet	0.45	0.30	0.15	0.45	0.42	0.15
Grey relational analysis	(0.83,0.93)	(0.86,0.93)	(0.83,0.93)	(0.83,0.98)	(0.86,0.96)	(0.83,0.98)

Table 3
Comprehensive index of evaluation obtained using L&G algorithm.

	Reconstruction similarity sub-index f_S	Confidence degree sub-index f_C	Edge form sub-index f_P	Comprehensive index f_{Idx}
Fig. 5(b)	0.863	0.722	0.446	0.278
Fig. 5(c)	0.874	0.729	0.451	0.287
Fig. 5(d)	0.877	0.729	0.460	0.294
Fig. 5(e)	0.882	0.706	0.949	0.591
Fig. 5(f)	0.887	0.713	0.955	0.604
Fig. 5(g)	0.895	0.715	0.967	0.619

results than that of the wavelet analysis. Therefore, the optimized parameters can be obtained by using the proposed edge detection evaluation index.

Three more typical ferrograph images are selected as the experimental images. Fig. 6(a) shows an image with a large abnormal wear particle and uneven background colour. Fig. 7(a) shows an image with wear debris distributed in the form of chains, and the background colour is almost green. Fig. 8(a) shows an image that has inconsistent background brightness and some black oxide particles with blurred edges. By using the same six groups of thresholds from Table 2, different edge images can be obtained, as shown in Figs. 6(b)–(g), 7(b)–(g), and 8(b)–(g). The comprehensive index of evaluation f_{Idx} is calculated and listed in Table 4 for obtaining the various edge detection results. The comprehensive index of evaluation f_{Idx} is also specified below each image.

It can be observed from Fig. 6(a) that because the large wear particle has a rough surface, the texture on the surface has been mistakenly detected as several false edges, as shown in Fig. 6(d) and (g). However, using the proposed algorithm, the obtained comprehensive index of the evaluation result is the same as that observed with human eyes, and the order of the quality of the evaluation result is

Fig. 6(f) > Fig. 6(e) > Fig. 6(c) > Fig. 6(b) > Fig. 6(g) > Fig. 6(d).

(a) Original image   (b) $f_{Idx} = 0.282$ (c) $f_{Idx} = 0.304$ (d) $f_{Idx} = 0.125$

(e) $f_{Idx} = 0.603$ (f) $f_{Idx} = 0.604$ (g) $f_{Idx} = 0.205$
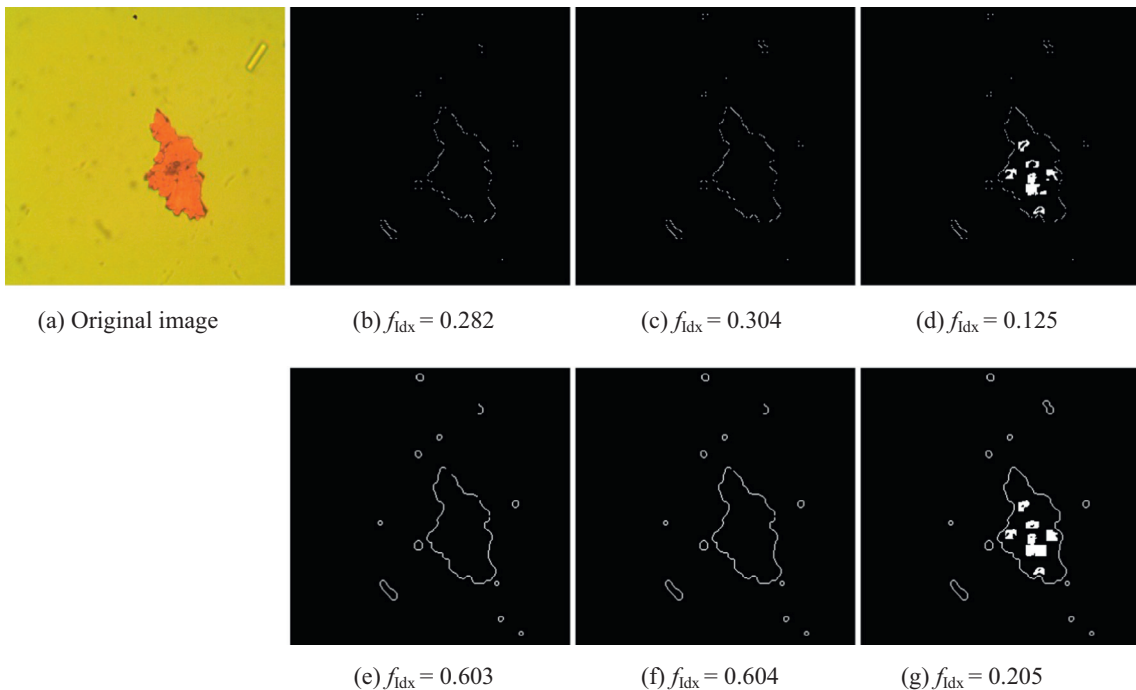
Fig. 6. Edge images of example 2 obtained with different parameter values.

(a) Original image   (b) $f_{Idx} = 0.07$ (c) $f_{Idx} = 0.077$ (d) $f_{Idx} = 0.078$

(e) $f_{Idx} = 0.16$ (f) $f_{Idx} = 0.167$ (g) $f_{Idx} = 0.177$
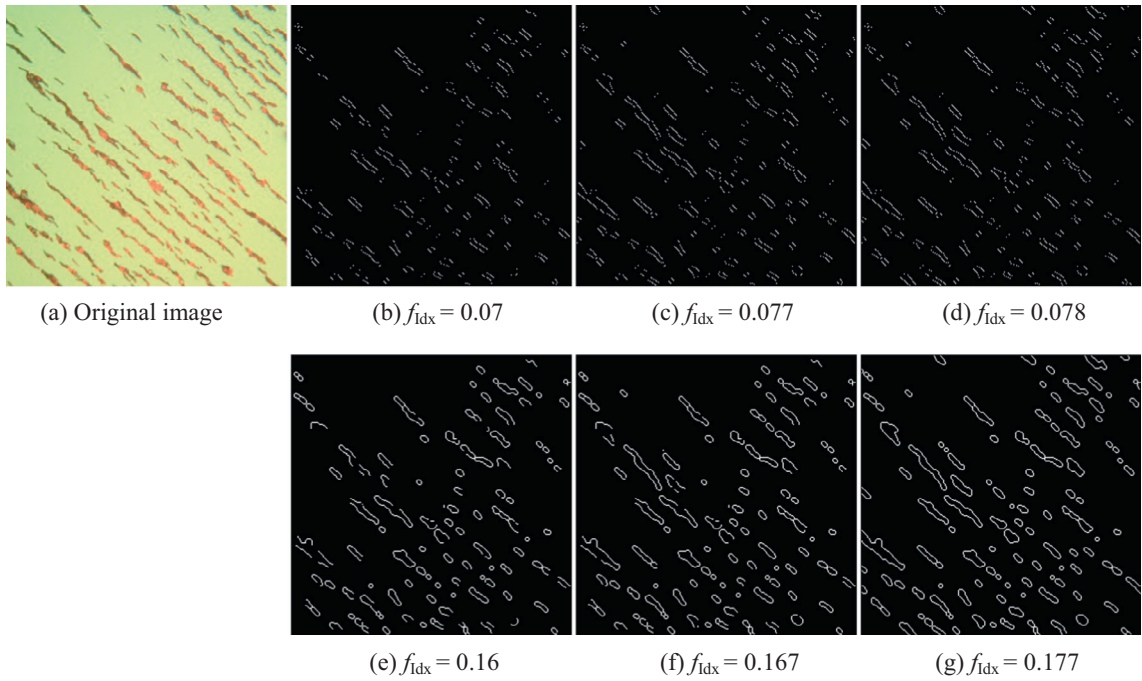
Fig. 7. Edge images of example 3 obtained with different parameter values.

(a) Original image   (b) $f_{Idx} = 0.213$ (c) $f_{Idx} = 0.228$ (d) $f_{Idx} = 0.235$

(e) $f_{Idx} = 0.551$ (f) $f_{Idx} = 0.570$ (g) $f_{Idx} = 0.605$
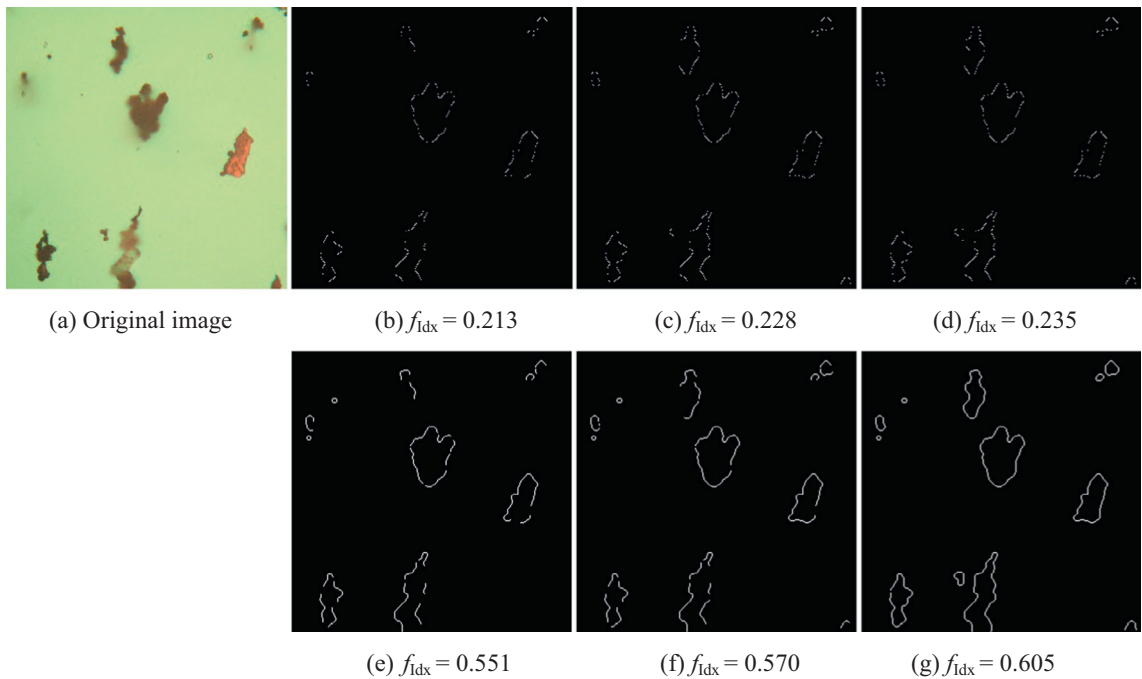
Fig. 8. Edge images of example 4 obtained with different parameter values.

Therefore, for this image, the best threshold would be that of group 5, i.e., (0.42, (0.86, 0.96)).

As shown in Fig. 7, because some of the fine wear debris is too tiny to be detected, each comprehensive index is small. However, according the order of the index, the optimized threshold, i.e., the sixth group of thresholds can be obtained.

Table 4
Comprehensive index of evaluation for L&G algorithm.

	Comprehensive index f_{Idx}		Comprehensive index f_{Idx}		Comprehensive index f_{Idx}
Fig. 6(b)	0.282	Fig. 7(b)	0.07	Fig. 8(b)	0.213
Fig. 6(c)	0.304	Fig. 7(c)	0.077	Fig. 8(c)	0.228
Fig. 6(d)	0.125	Fig. 7(d)	0.078	Fig. 8(d)	0.235
Fig. 6(e)	0.603	Fig. 7(e)	0.16	Fig. 8(e)	0.551
Fig. 6(f)	0.604	Fig. 7(f)	0.167	Fig. 8(f)	0.57
Fig. 6(g)	0.205	Fig. 7(g)	0.177	Fig. 8(g)	0.605

Fig. 8(a) shows some black oxide particles with blurred edges. By using the first five groups of thresholds, some edges of wear particles were lost owing to blurring as shown in Fig. 8(b)–(f). As can be seen from Fig. 8(g), the majority of the edges are closed, and its comprehensive index also confirms it to be the best edge detection result.

3.2. Evaluation of the various algorithms for edge detection

In this experiment, five detectors and algorithms, i.e., the Sobel, Roberts, Canny, lifting wavelet, and L&G algorithms are selected for detecting the edges of wear particles in Fig. 9(a). The detection results are shown in Fig. 9(b)–(f), and the comprehensive index is calculated and listed in Table 5 for evaluating the various edge detection results. The comprehensive index of evaluation f_{Idx} and the threshold parameter used in the L&G algorithm are also specified below each corresponding image.

It can be observed that there are some false edges and unclosed edges in Fig. 9(b), and the boundaries are not single-pixel-wide; Fig. 9(c) and (d) also have similar problems to those observed in Fig. 9(b). In Fig. 9(e), there are almost no false edges; however, the boundary is unclosed and not single-pixel-wide. These problems certainly affect the successive analysis of wear particles. Fig. 9(f) shows the best results of edge detection; the edges of the majority of the wear particles are closed and single-pixel-wide.

Table 5 shows the same order of the quality of the evaluation result that people observe, that is,

Fig. 9(f) > Fig. 9(e) > Fig. 9(d) > Fig. 9(c) > Fig. 9(b).

When the L&G algorithm is used to detect the edges of wear particles, the best edge detection results can be obtained, and the results of the lifting wavelet algorithm are slightly inferior. However, in the case of the Canny, Roberts, and Sobel algorithms, because they have no strong anti-noise ability, the result images have more false edges leading to edge detection quality is reduced.

(a) Original image   (b) Sobel f_{Idx} = 0.139   (c) Roberts f_{Idx} = 0.181

(d) Canny f_{Idx} = 0.251   (e) Lifting wavelet f_{Idx} = 0.326   (f) L&G f_{Idx} = 0.465 (0.1, (0.86, 0.96))
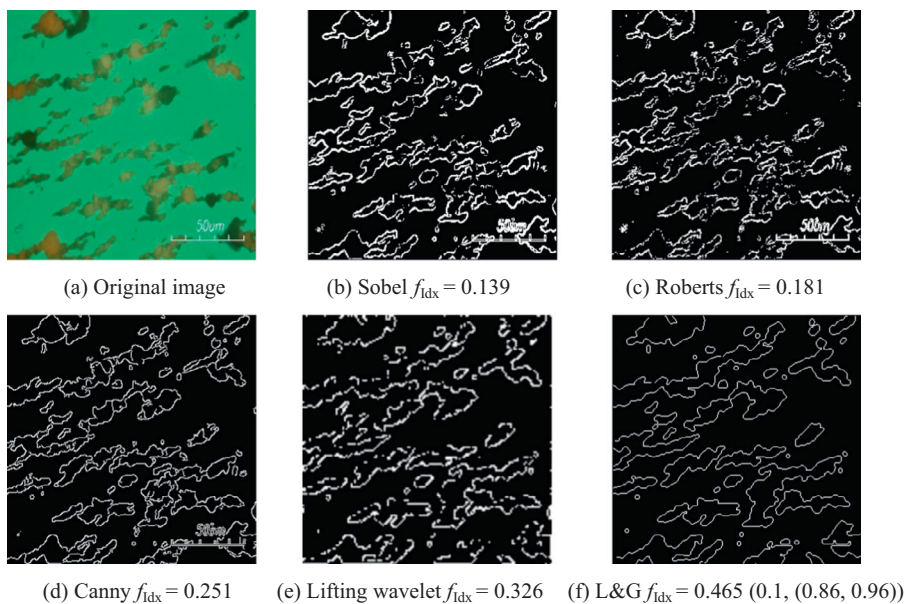
Fig. 9. Detection results of example 5 by various algorithms.

Table 5
Evaluation results of edge detection for various algorithms.

	Reconstruction similarity sub-index f_S	Confidence degree sub-index f_C	Edge form sub-index f_P	Comprehensive index f_{Idx}
Fig. 9(b)	0.967	0.297	0.483	0.139
Fig. 9(c)	0.963	0.303	0.620	0.181
Fig. 9(d)	0.965	0.280	0.930	0.251
Fig. 9(e)	0.949	0.394	0.873	0.326
Fig. 9 (f)	0.898	0.535	0.967	0.465

(a) Original image   (b) Sobel $f_{Idx} = 0.061$ (c) Roberts $f_{Idx} = 0.135$

(d) Canny $f_{Idx} = 0.244$ (e) Lifting wavelet $f_{Idx} = 0.355$ (f) L&G $f_{Idx} = 0.598$ (0.15, (0.83, 0.98))
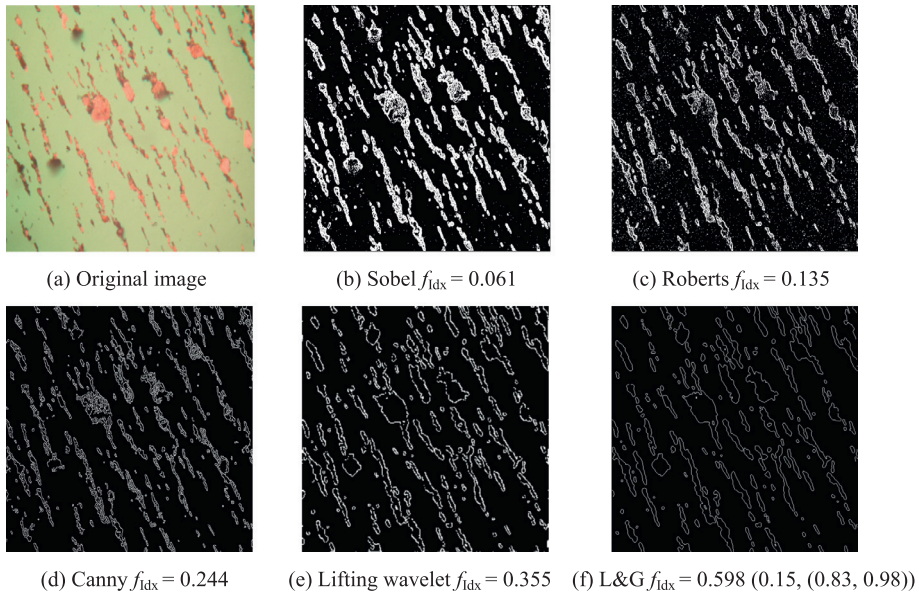
Fig. 10. Detection results of example 6 by various algorithms.

(a) Original image   (b) Sobel $f_{Idx} = 0.062$ (c) Roberts $f_{Idx} = 0.111$

(d) Canny $f_{Idx} = 0.282$ (e) Lifting wavelet $f_{Idx} = 0.354$ (f) L&G $f_{Idx} = 0.454$ (0.15, (0.83, 0.98))
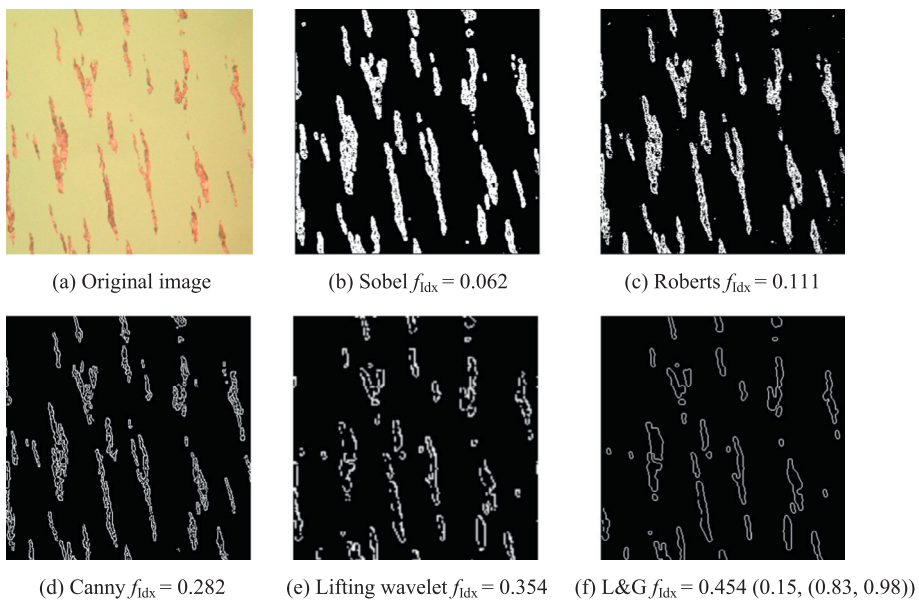
Fig. 11. Detection results of example 7 by various algorithms.

Table 6
Evaluation results of edge detection with various algorithms.

	Comprehensive index f_{Idx}		Comprehensive index f_{Idx}		Comprehensive index f_{Idx}
Fig. 10(b)	0.061	Fig. 11(b)	0.062	Fig. 12(b)	0.149
Fig. 10(c)	0.135	Fig. 11(c)	0.111	Fig. 12(c)	0.271
Fig. 10(d)	0.244	Fig. 11(d)	0.282	Fig. 12(d)	0.284
Fig. 10(e)	0.355	Fig. 11(e)	0.354	Fig. 12(e)	0.41
Fig. 10(f)	0.598	Fig. 11(f)	0.454	Fig. 12(f)	0.599

(a) Original image   (b) Sobel $f_{Idx} = 0.149$ (c) Roberts $f_{Idx} = 0.271$

(d) Canny $f_{Idx} = 0.284$ (e) Lifting wavelet $f_{Idx} = 0.41$ (f) L&G $f_{Idx} = 0.599$ (0.15, (0.83, 0.98))
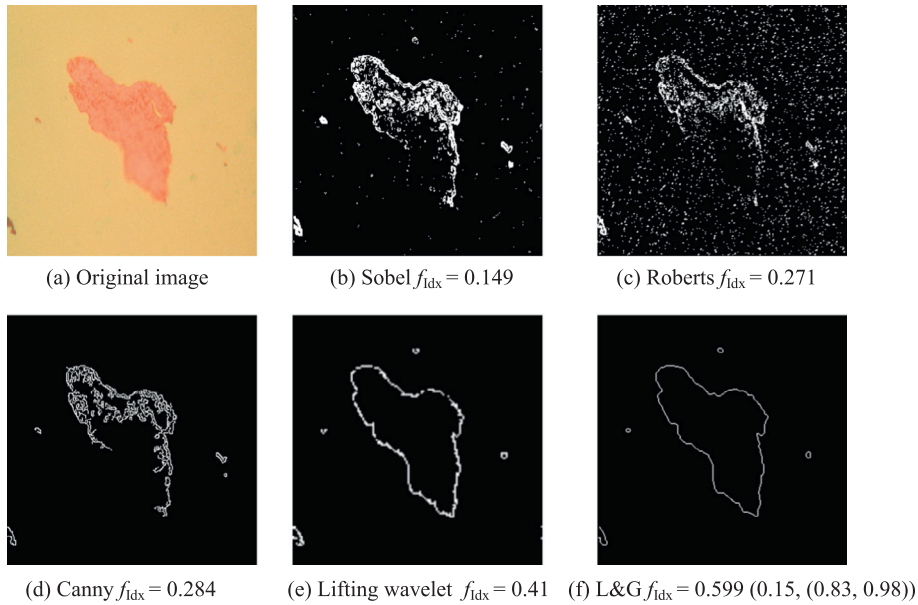
Fig. 12. Detection results of example 8 by various algorithms.

Another three typical ferrograph images are selected as experimental images. Fig. 10(a) shows an original ferrograph image that has uneven background brightness with some large wear particles and wear debris chains. Fig. 11(a) shows an original image that has a yellow background colour with some wear debris chains. Fig. 12(a) shows an image that has a fatigue wear particle with blurred edges. The detection results are shown in Figs. 10(b)–(f), 11(b)–(f), and 12(b)–(f), and the comprehensive index is calculated and listed in Table 6 for evaluating the various edge detection results. The comprehensive index f_{Idx} and the threshold parameter used in the L&G algorithm are also shown below each corresponding image.

The larger the comprehensive index, the better the edge detection obtained. As can be observed from Table 6, the best edge detection results are shown in Figs. 10(f), 11(f), and 12(f), which shows the same order of the quality of the evaluation result that people observe.

The above experimental results indicate that the proposed method is effective for evaluating the parameters and algorithm of edge detection for ferrograph images.

4. Conclusion

In this paper, a non-reference quantitative evaluation method for edge detection of wear particles is proposed. This method does not require an image edge reference or other prior knowledge. Firstly, the method can be used to reconstruct an image by using the improved interpolation algorithm based on psychological distance and to calculate the reconstruction similarity sub-index f_S between the reconstructed image and the original image. Secondly, the calculated confidence degree sub-index f_C is used to indicate the true or false degree of edge pixels. Thirdly, the calculated edge form sub-index f_P is used to indicate the direction consistency and width uniformity of the edges. Lastly, the final comprehensive evaluation index f_{Idx} was obtained from the calculated reconstruction similarity sub-index f_S, confidence degree sub-index f_C, and edge form sub-index f_P. From the preliminary experimental results, it could be observed that the evaluation result for the edge detection of wear particles obtained using the proposed method is similar to that observed with human eyes, and the evaluation results are objective and reasonable. The evaluation method has certain practical application value in an automatic ferrography analysis system. Furthermore, because of the various practical engineering applications, the wide variety of wear particle

types, various image processing and segmentation methods, etc., are likely to increase the complexity of the evaluation process. It is necessary that the proposed evaluation method be further discussed with respect to various practical environments in order to make the evaluation method more suitable for specific engineering applications.

Acknowledgments

References

[1] D. Scott, W.W. Seifert, V.C. Westcott, Ferrography—an advanced design aid for the 80's, Wear 1975 (34) (1975) 251–260.
[2] Y. Zhiyi, L. Yubin, C. Jian, Ferrography based on debris group theory and its application to machine failure prediction, Chin. J. Mech. Eng. 15 (2002) 25–28.
[3] M. Kumar, Advancement and current status of wear debris analysis for machine condition monitoring: a review, Indust. Lubr. Tribol. 65 (1) (2013) 3–11.
[4] B.J. Roylance, Ferrography—then and now, Tribol. Int. 38 (10) (2005) 857–862.
[5] S. Raadnui, Wear particle analysis—utilization of quantitative computer image analysis: a review, Tribol. Int. 38 (10) (2005) 871–878.
[6] X.P. Yan, C.H. Zhao, Z.Y. Lu, X.C. Zhou, H.L. Xiao, A study of information technology used in oil monitoring, Tribol. Int. 38 (10) (2005) 879–886.
[7] M.S. Laghari, Q.A. Memon, G.A. Khuwaja, Knowledge based wear particle analysis, Int. J. Inform. Technol. 1 (3) (2004) 91–95.
[8] U. Cho, J.A. Tichy, Quantitative correlation of wear debris morphology grouping and classification, Tribol. Int. 33 (2000) 461–467.
[9] V.D. Gonçalves, L.F.d. Almeida, and M.H. Mathias, Wear particle classifier system based on an artificial neural network, J. Mech. Eng. 56 (2010) 6.
[10] G.W. Stachowiak, P. Podsiadlo, Towards the development of an automated wear particle classification system, Tribol. Int. 39 (12) (2006) 1615–1623.
[11] J. Wang, X. Wang, A wear particle identification method by combining principal component analysis and grey relational analysis, Wear 304 (2013) 96–102.
[12] B.J. Roylance, I.A. Albidewi, M.S. Laghari, Computer-aided vision engineering (CAVE) - quantification of wear particle morphology, Lubr. Eng. 50 (2) (1994) 111–116.
[13] B.J. Roylance, I.A. Albidewi, A.R. Luxmoore, A.L. Price, The development of a computer-aided systematic particle analysis procedure-CASPA, Lubr. Eng. 48 (12) (1992) 940–946.
[14] T.P. Sperring, T.J. Nowell, SYCLOPS—a qualitative debris classification system developed for RAF early failure detection centres, Tribol. Int. 38 (10) (2005) 898–903.
[15] Z. Peng, S. Goodwin, Wear-debris analysis in expert systems, Tribol. Lett. 11 (3–4) (2001) 177–184.
[16] T.H. Wu, J.H. Mao, J.T. Wang, J.Y. Wu, Y.B. Xie, A new on-Line visual ferrograph, Tribol. Trans. 52 (5) (2009) 623–631.
[17] P. Podsiadlo, G.W. Stachowiak, Development of advanced quantitative analysis methods for wear particle characterization and classification to aid tribological system diagnosis, Tribol. Int. 38 (10) (2005) 887–897.
[18] Z. Peng, T.B. Kirk, Automatic wear particle classification using neural networks, Tribol. Lett. 5 (1998) 249–257.
[19] D. Ziou, S. Tabbone, Edge detection techniques: an overview, Int. J. Pattern Recogn. Image Anal. 8 (1998) 537–559.
[20] F.M. Chen, J.Q. Wang, L. Zhang, Edge detection of Ferrography image based on lifting wavelet(in Chinese), Mech. Sci. Technol. 32 (10) (2013) 1467–1471.
[21] D. Feng, B. Zhang, X. Wang, A novel operator based on grey relational analysis, ICIEA 2009 (2009) 2686–2689.
[22] J. Wang, L. Zhang, F. Lu, X. Wang, The segmentation of wear particles in ferrograph images based on an improved ant colony algorithm, Wear 311 (1–2) (2014) 123–129.
[23] S. Nercessian, K. Panetta, S. Agaian, a non reference measure for objective edge map evaluation, in: Proceedings of the 2009 IEEE International Conference on Systems, Man, and Cybernetics. San Antonio, TX, USA, 2009.
[24] Y. Yitzhaky, A method for objective edge detection evaluation and detector parameter selection, IEEE Trans. Pattern Anal. Mach. Intell. 25 (10) (2003) 1–7.
[25] S.C. Nercessian, S.S. Agaian, K.A. Panetta, A new reference-based measure for objective edge map evaluation, in: Proc. SPIE 7351, Mobile Multimedia/Image Processing, Security, and Applications 2009, 2009, pp. 7351.
[26] K. Panetta, C. Gao, S. Agaian, S. Nercessian, Nonreference medical image edge map measure, Int. J. Biomed. Imag. 2014 (2014) 931375.
[27] S. Carlsson, Sketch based coding of grey level images, Signal Proces. 15 (1) (1988) 57–83.
[28] B. Govindarajani, K. Panett, S. Agaian, Progressive edge detection on multi-bit images using polynomial-based binarization, in: IEEE International Conference on Machine, Learning and Cyber., Kunming, China, July 2008, 2008, pp. 3714–3719.
[29] B. Govindarajan, K.A. Panetta, S. Agaian, Image reconstruction for quality assessment of edge detectors, in: 2008 IEEE International Conference on Systems, Man and Cybernetics (SMC 2008), 2008, pp. 691–696.
[30] R.N. Shepard, Toward a universal law of generalization for psychological science, Science 237 (4820) (1987) 1317–1323.
[31] L.H. Jin, D.H. Li, X.Z. Yao, Adaptive distand-weighted median filtering algorithm(In Chinese), Pattern Recogn. Artif. Intel. 20 (4) (2007) 577–581.
[32] Z. Wang, A.C. Bovik, H.R. Sheikh, E.P. Simoncelli, Image quality assessment from error visibility to structural similarity, IEEE Trans. Image Process. 13 (4) (2004) 1–14.
[33] Q. Zhu, Efficient evaluations of edge connectivity and width uniformity, Image Vis. Comput. (1996) 21–34.
[34] F.M. Chen, Research on edge detection of wear particle by combining lifting wavelet and grey relational analysis (in Chinese), Master Thesis, Nanjing University of Aeronautics and Astronautics, 2013.